Journal of the European Ceramic Society **11** (1993) 241–251

Experimental Investigation of the Zr–B–Cl–H CVD System

A. Wang & G. Malé

Institut de Science et de Génie des Matériaux et Procédés, BP No. 5, Odeillo, 66120 Font-Romeu, France

(Received 8 June 1992; revised version received 10 July 1992; accepted 13 July 1992)

Abstract

The Zr–B–Cl–H system was experimentally studied by LPCVD using gas mixtures of BCl_3, $ZrCl_4$ and H_2.

A rational experimental design was adopted and the results showed that the deposition rate and the surface morphology depended strongly on the reduction of boron trichloride by hydrogen.

The kinetics were detailed and a deposition diagram was established. The experimental diagram is in good agreement with the thermodynamic predictions.

From the characterization of deposits it resulted that zirconium diboride is the only compound which can be synthesized in the system. Depending on the experimental conditions, it can either crystallize in isotropic form or in three types of textures, and can either be accompanied by free boron or not. It also showed the existence of an amorphous domain which is constituted by boron with a small quantity of zirconium (<5%).

Das Zr–B–Cl–H System wurde ausgehend von Gasmischungen von BCl_3, $ZrCl_4$ und H_2 mittels LPCVD untersucht.

Durch Anwendung einer rationellen Versuchsanordnung konnte gezeigt werden, daß die Abscheidungsgeschwindigkeit und die Oberflachenmorphologie in starken Maße von der Reduktion von Bortrichlorid durch Wasserstoff abhängig sind.

Die Kinetik wird ausfurlich dargestellt und ein Abscheidungsdiagram erstellt, welches in guter Übereinstimmung mit thermodynamischen Betrachtungen ist.

Aus der Charakterisierung der Abscheidungsprodukte folgt, daß Zirkoniumdiborid als einzige Verbindung in diesem System erhalten werden kann. In Abhängigkeit von den experimentellen Bedingungen kristallisiert die Substanz entweder in einer isotropen Form oder in drei Texturtypen und unter bestimmten Umständen kann nebenbei elementares Bor auftreten.

Die Existenz einer amorphen Domäne aus Bor mit einem geringen Anteil von Zirkonium (<5%) wurde ebenfalls nachgewiesen.

Une exploration paramétrique du système Zr–B–Cl–H est effectuée sous pression réduite à partir de mélanges de BCl_3, de $ZrCl_4$ et de H_2.

Un plan d'expérience rationnel montre que la vitesse de dépôt et la morphologie de surface des couches obtenues dépendent étroitement de la réduction de BCl_3 par l'hydrogène.

La cinétique a été précisée, et un diagramme de dépôt a été établi. Ce dernier est en bon accord avec les prévisions thermodynamiques.

De la caractérisation des dépôts, il ressort que le seul composé synthétisé est le diborure de zirconium. Suivant les conditions paramétriques, il peut cristalliser de façon isotrope ou présenter trois types de textures et être accompagné ou non de bore libre en plus ou moins grande quantité.

Un domaine amorphe constitué de bore contenant moins de 5% de zirconium a également été mis en évidence.

1 Introduction

Zirconium diboride has a great potential application in many domains because of its good chemical, electrical and optical properties. Interest in this compound has increased and a number of studies have been done, especially on sintered materials.

Already, in 1931, Moers[1] successfully synthesized zirconium diboride from a mixture of boron tribromide and zirconium tetrachloride reduced by hydrogen. The few CVD studies, often at 1 atm, only started after 1975. Zirconium chloride ($ZrCl_4$) and boron chloride (BCl_3) were generally used in a reducing hydrogen flow.

The flow control of zirconium tetrachloride, solid precursor, is not easy. $ZrCl_4$ was often prepared *in*

Journal of the European Ceramic Society 0955-2219/93/$6.00

situ by chlorination of sponge zirconium.[2-4] Vapour transport by hydrogen flow through the heated chloride was also used.[5]

Recently, zirconium borohydride was used for synthesizing the boride at low temperature,[6-8] but this single precursor of zirconium and boron is not commercialized and its use is not easy.

In all studies only zirconium diboride was synthesized, sometimes accompanied by free boron. The deposition rate increased with temperature. Randich[2] observed that the deposition rate increased with $BCl_3/ZrCl_4$ ratio and decreased with H/Cl ratio. In contrast, other authors[4] indicated that hydrogen had a strongly positive influence on deposition rate.

Few layer microstructures were given. A preferred orientation, in which the *c*-direction of the ZrB_2 crystal cell was parallel to the substrate surface, was observed.[4,5] The authors observed also a very good adherence of the ZrB_2 layer to graphite, tantalum and copper.

This work contributes to the experimental study of the system, using the same precursors (BCl_3, $ZrCl_4$, H_2) but at low pressure. It is in the wake of a thermodynamic approach[9] which shows particularly the strong influence of BCl_3 reduction by hydrogen on the nature of the condensed phase and on the yield, as well as the preponderance of ZrB_2 deposit over the other possible compounds (ZrB, ZrB_{12}). According to this study, the solid yield increased firstly with temperature, secondly and especially with hydrogen content, but decreased with pressure.

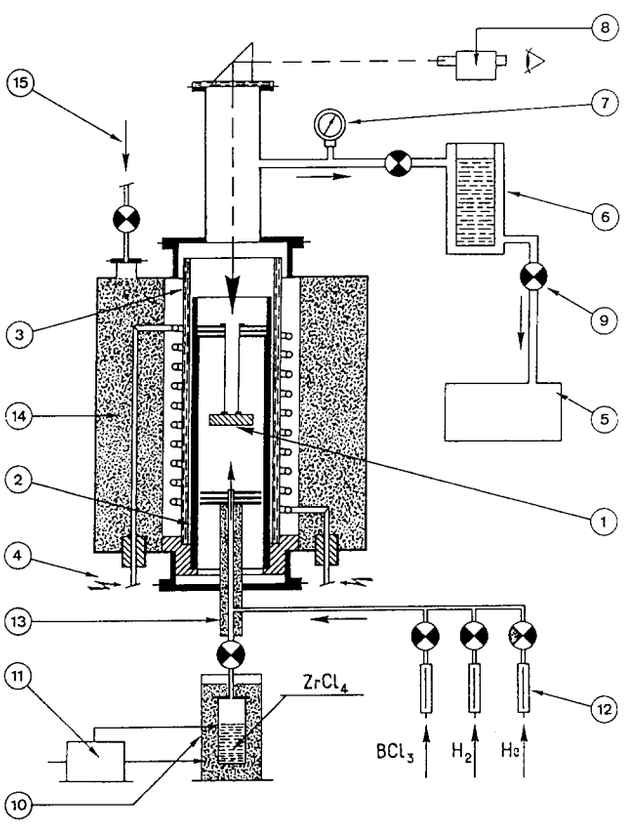

Fig. 1. Schematic diagram of the apparatus. 1, Substrate; 2, graphite tube; 3, quartz tube; 4, inductor; 5, vacuum pump; 6, cryotrap; 7, manometer; 8, optical pyrometer; 9, valve; 10, isothermic furnace; 11, temperature regulator; 12, flow meter; 13 and 14, thermal insulation; 15, access to vacuum pump.

2 Experimental Procedure

The apparatus used in this work is a hot-wall CVD reactor, schematically shown in Fig. 1.

Zirconium chloride is contained in a thermostated vaporizer and evaporated above 470 K through an orifice 1 mm in diameter.

The substrates are pure graphite (CWA manufactured by Vicarb, Grenoble, France) disks of 16 mm in diameter and 5 mm thick. The surfaces are polished with diamond paste to 6 μm and washed ultrasonically in ethanol.

The purity of the gas used is superior to 99·99% except for $ZrCl_4$ (>98%).

The deposits are examined with different techniques: X-ray diffraction, optical metallography, scanning electron microscopy (SEM), electron microprobe analysis, Auger electron spectrography (AES), microhardness and roughness measurements.

3 Experimental Design

For a complex chemical system which has a number of parameters it is suitable to use a rational methodology which permits a maximum amount of information concerning the influence of the diverse parameters in the answer to be obtained with a small number of experiments.

3.1 Application to the $ZrCl_4$–BCl_3–H_2 system

There are five independent parameters in the system: temperature (T), total pressure (P_T) and three gas fluxes—$D\mathrm{ZrCl_4}$, $D\mathrm{BCl_3}$, $D\mathrm{H_2}$. In this case a fractional experimental design is adopted. This plan consists of only 16 experiments instead of 32, and gives a polynome with 16 terms.

The experimental design and the mathematical treatment of the results have been realized with a computer program, 'NEMROD', developed by Phan-Tan-Luu and coworkers.[10]

The two levels, maximum (+) and minimum (−) for each parameter, which fix the experimental

Table 1. Parametric domain of the experimental design

Parameters	−	+
T (K)	1323	1473
P (Pa)	10^3	5×10^3
$D\mathrm{ZrCl_4}$ (litre.h^{-1})	0·05	0·8
$D\mathrm{BCl_3}$ (litre.h^{-1})	0·12	3·0
$D\mathrm{H_2}$ (litre.h^{-1})	1·0	10·0

Table 2. Experimental design

Number	T	P	$DZrCl_4$	$DBCl_3$	DH_2
1	−	−	−	−	−
2	+	−	−	+	+
3	−	+	−	+	−
4	+	+	−	−	+
5	−	−	+	−	+
6	+	−	+	+	−
7	−	+	+	+	+
8	+	+	+	−	−
9	−	−	−	+	+
10	+	−	−	−	−
11	−	+	−	−	+
12	+	+	−	+	−
13	−	−	+	+	−
14	+	−	+	−	+
15	−	+	+	−	−
16	+	+	+	+	+

domain, are given in Table 1. The choice is based on the preliminary test, on the thermodynamic studies,[9] and on the limits of the apparatus used in this work.

The experimental matrix at two levels (+, −) is given in Table 2.

3.2 Exploitation of the experimental design

Among the quantitative responses of interest in the work are deposition rate and arithmetic roughness (*Ra*), which give an image of the deposit microstructure.

In Table 3 these results and the morphological and structural observations for the 16 experiments predicted by the experimental design are given. The mathematical treatment of the results leads to a polynomial response modelling.

3.2.1 Deposition rate

Because of the hydrodynamic inhomogeneity, the deposition rate on the front face towards the gas flux is different from that on the back face away from the flux. Consequently, the values given in Table 3 correspond to the deposition rate on the face towards the flux. The mathematical treatment leads to the following deposition model:

$$\begin{aligned} V(\mu\text{m}.\text{h}^{-1}) = {} & 29{\cdot}55 + 27{\cdot}2D\text{H}_2 + 25{\cdot}08D\text{BCl}_3 \\ & + 23{\cdot}12(D\text{H}_2 . D\text{BCl}_3) \\ & + 17{\cdot}22(D\text{H}_2 . P_\text{T}) + 16{\cdot}25D\text{ZrCl}_4 \\ & + 15{\cdot}28P_\text{T} + 14{\cdot}7(D\text{H}_2 . D\text{ZrCl}_4) \\ & + 6{\cdot}18(T . D\text{BCl}_3) + 5{\cdot}38(T . D\text{ZrCl}_4) \\ & + 5{\cdot}02T \end{aligned}$$

According to this polynome, the influence of parameters on the deposition rate, in order of importance, can be established as $D\text{H}_2$, $D\text{BCl}_3$, $D\text{ZrCl}_4$, P_T and T.

The larger coefficients for H_2, BCl_3 and their coupling show their strong influence, and demonstrate that the boron chloride reduction by hydrogen dominates the deposition rate.

Among all the parameters, the temperature has the weakest influence on the deposition rate, which can be explained by its small experimental range and by the existence of a diffusional process.

3.2.2 Surface roughness

The arithmetic roughness of deposit surface varies from 0·3 to 2·9 μm and shows a great difference of crystallization or microstructure. The mathematical treatment of the values concerned gives a polynome:

$$\begin{aligned} Ra(\mu\text{m}) = {} & 0{\cdot}94 + 0{\cdot}36D\text{BCl}_3 + 0{\cdot}33D\text{H}_2 \\ & + 0{\cdot}31(P_\text{T} . D\text{BCl}_3) + 0{\cdot}26(T . D\text{BCl}_3) \\ & + 0{\cdot}19P_\text{T} + 0{\cdot}12(T . D\text{ZrCl}_4) \\ & + 0{\cdot}094(P_\text{T} . D\text{ZrCl}_4) + 0{\cdot}081(T . D\text{H}_2) \\ & + 0{\cdot}081(D\text{ZrCl}_4 . D\text{BCl}_3) + 0{\cdot}056D\text{ZrCl}_4 \end{aligned}$$

Table 3. Results of the experimental design

Number	*Size of crystals*	*Phases*	*Textures* (δ_c)[a]	*Deposition rate* ($\mu m . h^{-1}$)[b]	*Rugosity* (*Ra*) (μm)
1	—	Amorphous	—	0·55	0·9
2	Small	ZrB_2	Isotropic	48·0	1·6
3	—	Amorphous	—	0·1	1·5
4	Small	ZrB_2	Isotropic	1·2	0·4
5	Small	ZrB_2	Isotropic	3·0	1·1
6	Medium	ZrB_2	Type II (0°–18°)	15·5	0·5
7	Large	ZrB_2	Type I (0°)	138·5	1·6
8	No deposit	—	—	—	0·1
9	Small	ZrB_2	Type III (53·4°)	35·0	0·8
10	Small	ZrB_2	Isotropic	1·0	0·3
11	Small	ZrB_2	Isotropic	19·0	1·3
12	—	Amorphous	—	1·5	1·2
13	Small	ZrB_2	Isotropic	0·1	0·3
14	Medium	ZrB_2	Type II (0°–18°)	11·0	0·5
15	No deposit	—	—	—	0·1
16	Large	ZrB_2	Type I (0°)	198·3	2·9

[a] δ_c = Angle between the *c*-axis and the substrate surface.
[b] Thicknesses on the face against the flux.

For the roughness, the influence of the parameters is in the following order: $D\mathrm{BCl_3}$, $D\mathrm{H_2}$, P_T, $D\mathrm{ZrCl_4}$. As for the deposition rate, the influence of all the parameters is positive for the roughness.

The flux of BCl_3 and H_2 always have great influence on the roughness of the surface and on the growth rate of the deposit.

The effect of total pressure on the crystalline growth is relatively smaller. The temperature, which weakly affects the deposition kinetics, has practically no influence on the roughness. It is probable that the narrow experimental temperature range (~200 K) does not permit the observation of its direct effect on the structure.

Generally, the results show the strong relation between kinetics and the crystalline size.

4 Parametric Kinetics Studies

Supplementary parametric studies based on the results of experimental design have been done. The temperature range, which seems too narrow in the experimental design, has been expanded. The influence of BCl_3 and H_2, the parameters with greater influence, has been examined and expressed in H/Cl and $BCl_3/ZrCl_4$ ratios.

4.1 Influence of temperature

Figure 2 shows the evolution of deposition rate versus temperature. The result is obtained under the following conditions: total pressure $P_T = 10$ mbar, total gas flow $D_T = 12$ litre . h^{-1}; gas ratios H/Cl = 4·5 and $BCl_3/ZrCl_4 = 2{\cdot}5$.

The deposition rate increases with temperature up to 1450 K. Above this temperature it is stabilized and decreases slowly.

Figure 3 gives the results in the form of an Arrhenius diagram. There exists a change in the slope at about 1170 K, which indicates a change in the deposition mechanism. The activation energy is

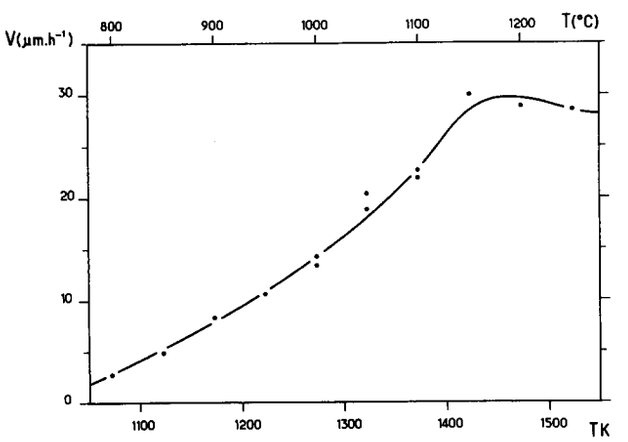

Fig. 2. Deposition rate versus temperature. $P_T = 10^3$ Pa, H/Cl = 2·5, B/Zr = 4·5, $D_T = 12$ litre . h^{-1}.

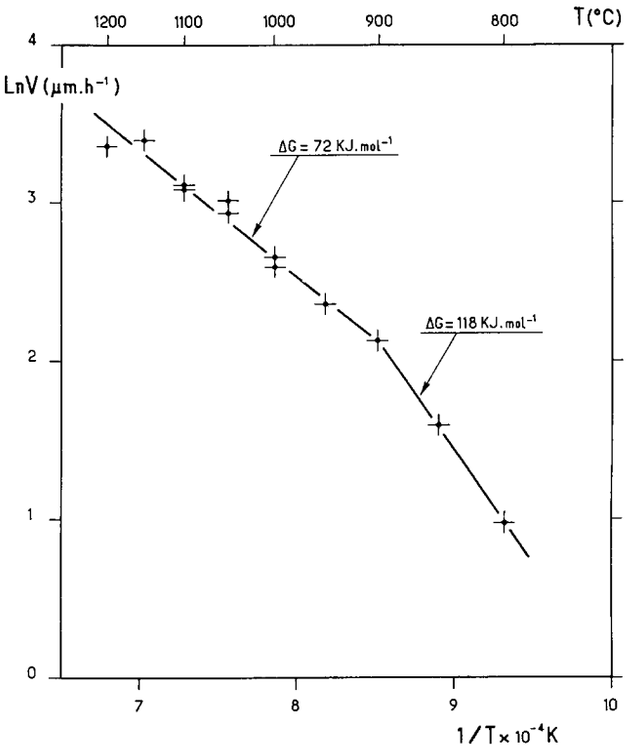

Fig. 3. Arrhenius diagram of the growth rate.

118 kJ . mol^{-1} for the temperature below 1170 K and 72 kJ . mol^{-1} for higher temperatures. The last value is in agreement with that obtained by Randich under an atmospheric pressure (66 kJ . mol^{-1}).[2]

4.2 Influence of hydrogen concentration

Figure 4 gives the deposition rate versus H/Cl ratio. The temperature is fixed at 1373 K, the pressure is 10^3 Pa and the $BCl_3/ZrCl_4$ ratio is 6·6.

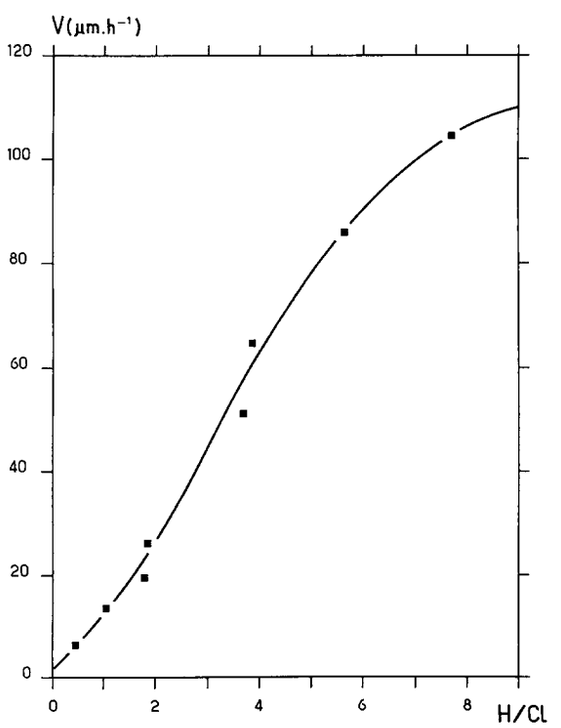

Fig. 4. Deposition rate versus hydrogen concentration. T = 1373 K, $P_T = 10^3$ Pa, B/Zr = 6·6.

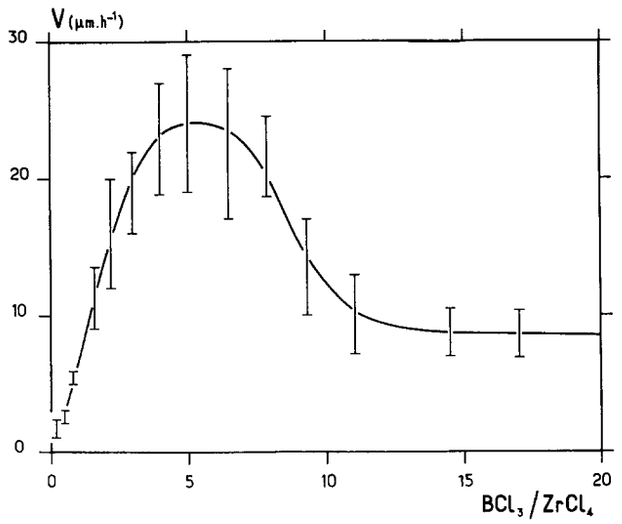

Fig. 5. Deposition rate versus $BCl_3/ZrCl_4$ molar ratio. $T = 1373$ K, $P_T = 10^3$ Pa, H/Cl = 2, $DZrCl_4 = 0{\cdot}45$ litre.h^{-1}.

The deposition rate is clearly more influenced by the hydrogen concentration in the gas mixture than by the temperature. In fact, the deposition rate increases very rapidly with the H/Cl ratio at first, then it seems to tend to be saturated.

This strong influence of hydrogen on kinetics is in good agreement with the thermodynamic approach,[9] and with the results of the experimental design.

4.3 Influence of BCl_3 concentration

Figure 5 shows the influence of the initial $BCl_3/ZrCl_4$ ratio on the deposition rate in the case of H/Cl = 2.

The deposition rate increases very rapidly at first with $BCl_3/ZrCl_4$ ratio, then decreases. For the ratio from 13 up to 200 (the diagram in Fig. 5 is cut at $BCl_3/ZrCl_4 = 20$), the deposition rate is stabilized at about 9 μm.h^{-1}. The maximum deposition rate is situated at $BCl_3/ZrCl_4 = 5$.

Other authors have observed the same phenomena in a cold-wall reactor, but the maximum position is situated at values (1·8–4·0) inferior to the present results. The difference in experimental, notably hydrodynamic conditions, can explain the discrepancy.

5 Characterization of the Deposited Solid

5.1 Experimental deposition diagram

A large number of deposit characterizations have permitted the building up of a diagram giving the existence domain of different deposited solids. Figure 6 shows the diagram established under the conditions: $T = 1373$ K, $P_T = 10$ mbar, $0{\cdot}2 < H/Cl < 40$, $0{\cdot}2 < BCl_3/ZrCl_4 < 200$.

This diagram is in good agreement with the

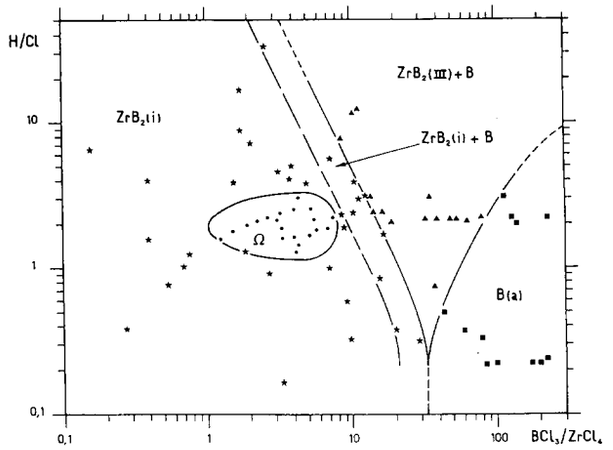

Fig. 6. Experimental deposition diagram of system Zr–B–Cl–H. $T = 1373$ K, $P_T = 10^3$ Pa. ★, Isotropic ZrB_2; ●, type I + II textured ZrB_2 (Ω); ▲, type III textured ZrB_2; ■, amorphous alloys.

theoretical diagram (Fig. 7) based on thermodynamic studies[9] and established under the same conditions. Only the domains corresponding to Zr and ZrB, difficult to access by experiment, have not been exploited.

The morphological, chemical and crystallographic aspects of the deposits, which permitted the building up of this diagram, will be discussed in the following sections.

5.2 X-Ray diffraction analysis

5.2.1 Phase identification

The analysis by X-ray diffraction indicates the existence of amorphous or well-crystallized deposits. In the latter case, only zirconium diboride (ZrB_2) is

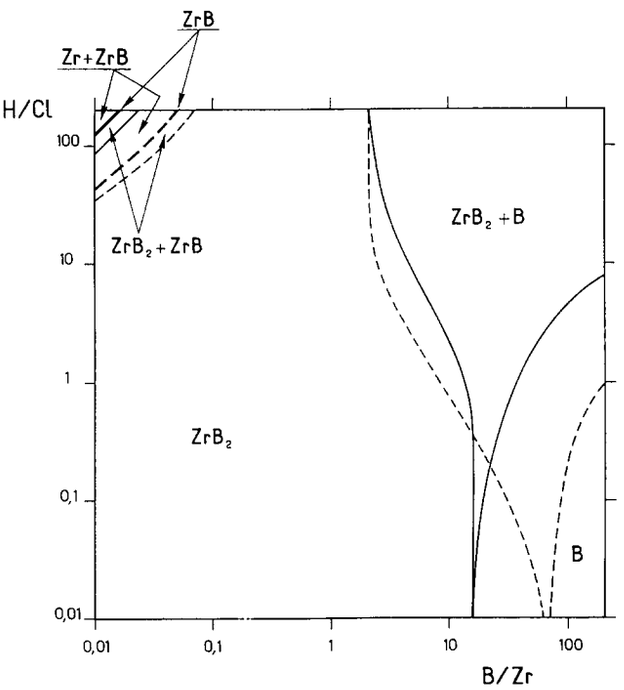

Fig. 7. Theoretical deposition diagram of system Zr–B–Cl–H. $T = 1400$ K; ——, $P_T = 10^5$ Pa; – – –, $P_T = 10^3$ Pa.

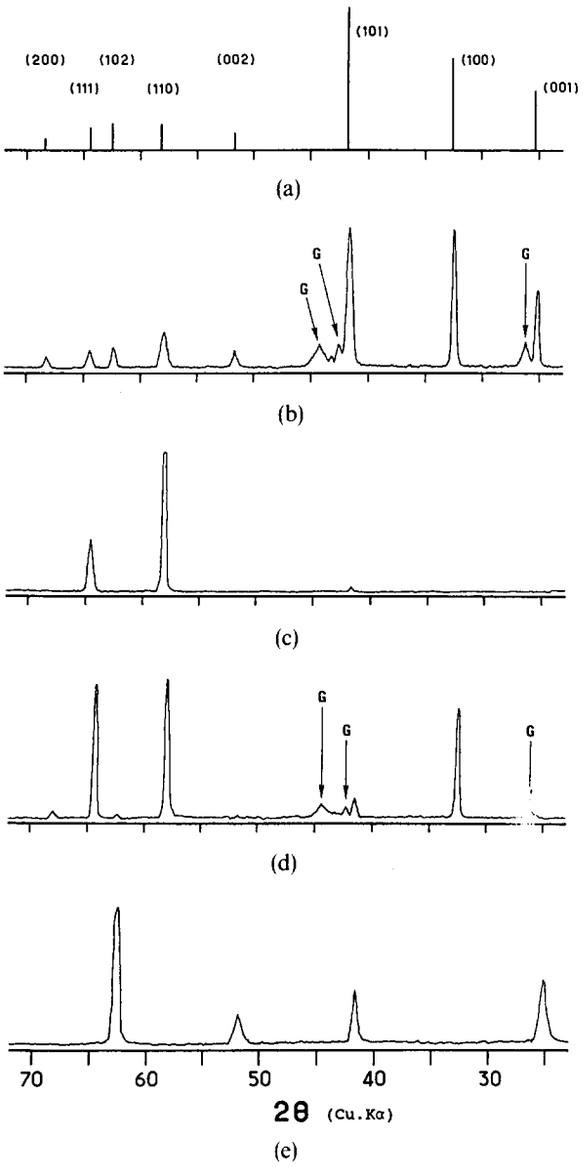

Fig. 8. Typical X-ray diffraction spectra of ZrB_2 deposit for different textures. G: Graphite of substrate. (a) Powder diagram; (b) isotropic; (c) type I; (d) type II; (e) type III.

identified. This phase occupies a large domain in the diagram (Fig. 6). In the other parts of the diagram the deposit is amorphous. Important intensity change in the diffraction peaks, which denotes the presence of preferred orientation, is observed.

Figure 8 shows some typical spectra. Spectrum A represents a standard powder diagram (ASTM Card No. 6-0610). Spectrum B indicates a deposit without a preferred orientation. The other three are representative of crystallites with different preferred orientations.

In the ZrB_2 monophase domain, the spectra have very sharp peaks which indicate a well-crystallized material.

5.2.2 Textures

The direction of preferred orientation is determined by a radiocrystallographic method with a cylindrical camera chamber.[11] In this work the orientation direction is represented by a symbol δ_c, which gives an angle between the c-axis of the hexagonal lattice of diboride and the substrate surface.

The preferred orientation of the deposit is very variable according to the experimental conditions. They can be classed in three types. Figure 9 shows the typical texture micrographs of these three types and their morphologies.

—Type I: The preferred orientation follows the plane (110) corresponding to $\delta_c = 0$, that is the c-axis of the crystallites is parallel to the substrate surface (Fig. 8(c), Fig. 9(a)). The rapid epitaxial growth forms good crystals.

—Type II: In this group there exists, in addition to the preceding direction, a range of preferred orientations, in which the angle δ_c varies from 11° to 21°. Figure 9(b) represents this type for $\delta_c = 18°$, corresponding to the diffraction spectrum (Fig. 8(d)).

—Type III: This groups together the orientations following the planes (113), (114), (115), (013), (015), etc., corresponding to the large angle δ_c (from 50° to 70°). Figure 9(c) is a typical example, and the corresponding morphology for a deposit has a preferred orientation angle $\delta_c = 53{\cdot}4°$, and its X-ray spectrum is shown in Fig. 8(e).

Types I and II (zero/small angle δ_c) coexist, type I being major in the monophasic domain signified by Ω in the deposition diagram (Fig. 6).

Type III (large δ_c) exists in an important domain: ZrB_2(III) + B in the diagram. The diffraction peaks (Fig. 8(e)) are broader than that of monophase diboride, which indicates a strong diminution of the crystallite size. The typical morphology of this type is shown in Fig. 9(c).

5.3 Element analysis

5.3.1 Composition

The element content has been determined by electron microprobe analysis. The deposited layers have homogeneous composition with a high purity; no elements other than zirconium and boron were detected. Figure 10 shows a linescan analysis of the elements Zr and B traversing a layer cross-section.

In contrast to temperature and pressure, the relative concentration of BCl_3 and $ZrCl_4$ in the input has a large influence on the deposited solid composition. This influence is illustrated by Fig. 11.

The analysis is made on the deposits situated on the line H/Cl = 2 in Fig. 6, which crosses the deposition diagram.

When the $BCl_3/ZrCl_4$ ratio is below 10, the obtained solid is always stoichiometric zirconium diboride (B/Zr(s) = 2). For a ratio above 10, free

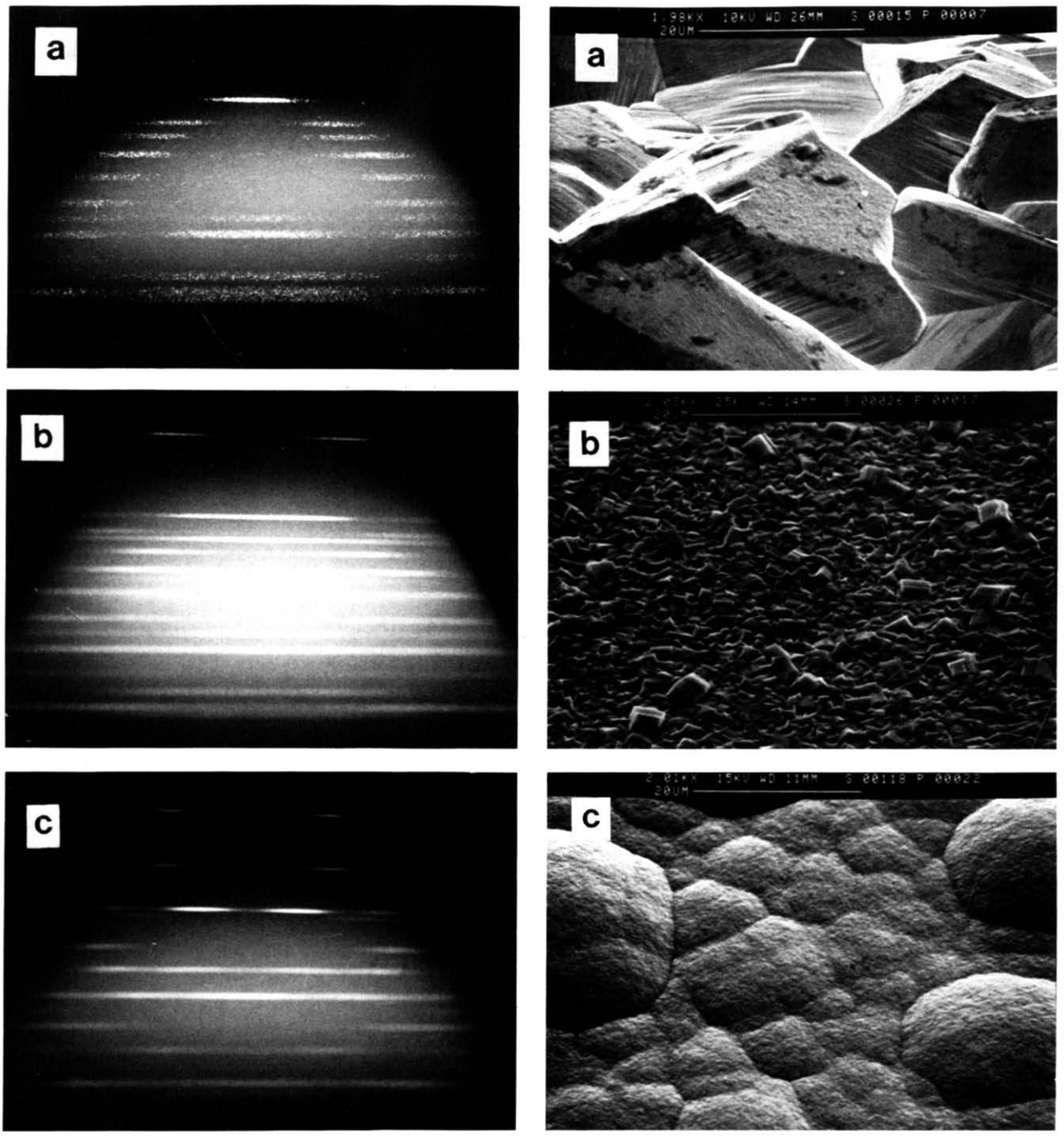

Fig. 9. Texture diagrams and corresponding morphologies. (a) Type I; (b) type II; (c) type III.

boron is codeposited with isotropic ZrB_2 or with type III oriented ZrB_2 to form the biphasic domain. The transition position of the monophasic–biphasic varies with the H/Cl ratio.

The boron content in the deposited solid increases rapidly with the $BCl_3/ZrCl_4$ ratio, particularly approaching the domain B(a). In this domain there is always more than 95 mol% boron in the deposited solid. In contrast to the crystallized pure boron obtained at the same temperature from the mixture of BCl_3 and H_2,[12] these deposits are amorphous. It is evident that the addition of $ZrCl_4$ modified the system and affected the solid crystallization.

The curve of Fig. 11 permits the more accurate determination of the limit position between the monophasic and biphasic domains for $H/Cl = 2$. This boundary is closer to the frontier F_1 ($BCl_3/ZrCl_4 = 6$) determined by theoretical studies (Fig. 7) than to the frontier F_2 ($BCl_3/ZrCl_4 = 15$) obtained by X-ray diffraction (Fig. 6). So there exists a small biphasic zone in which diboride is isotropic (domain $ZrB_2(i) + B$ in Figs 6 and 11).

5.3.2 Qualitative analysis

AES analyses have been performed in order to complement the microprobe ones.

The displacement and deformation of the characteristic zirconium and boron peaks are significant for their strong bonding in the ZrB_2 compound.

The AES spectra of four samples with different

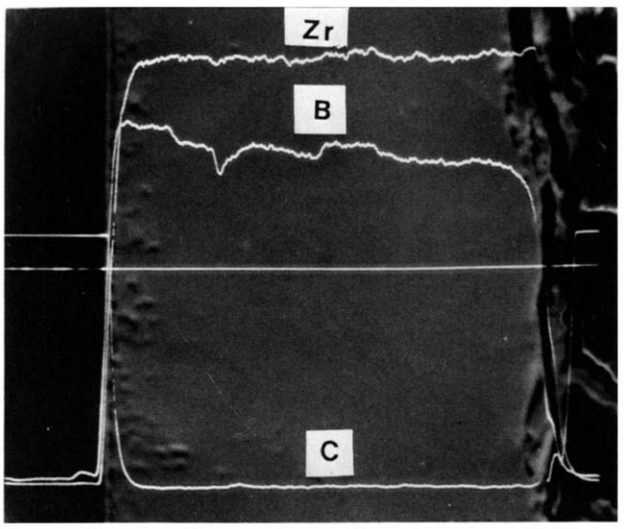

Fig. 10. Elemental analysis traversing a deposit section.

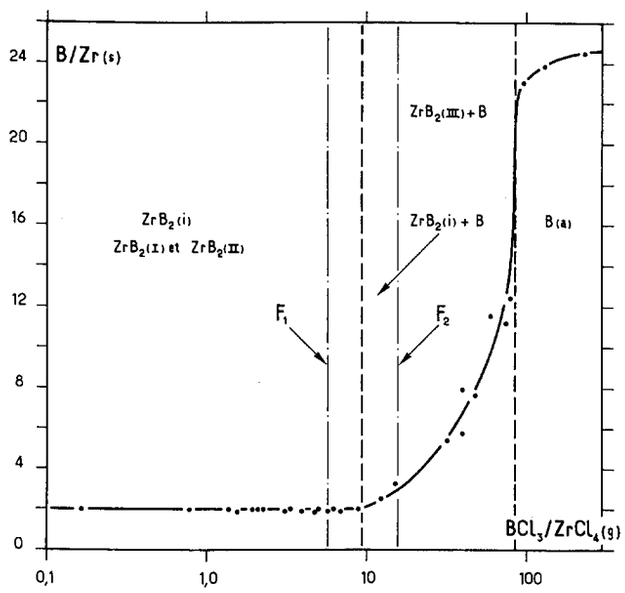

Fig. 11. Deposit composition (B/Zr) versus $BCl_3/ZrCl_4$ ratio. $T = 1373$ K, $P_T = 10^3$ Pa, H/Cl = 2. F_1: Theoretical frontier (Fig. 7). F_2: Experimental frontier (X-ray).

compositions (B/Zr = 2, 7·5, 11·5, 24·5), determined from microprobe analysis, are superimposed in Fig. 12 and compared with that of pure boron. When the B/Zr ratio increases, the *KLL* boron transition shifts progressively towards the position and shape of pure boron.

X-Ray diffractograms show only the ZrB_2 compound for all samples. So it is assumed that excess boron exists in amorphous form, just like in the boron-rich (B(a)) domain.

5.4 Surface morphology

The sample surfaces, observed by scanning electron microscopy, present a large feature diversity. This internal organization image of the layer is strongly linked to the deposition conditions.

Morphology of isotropic deposits in the monophasic domain ZrB_2 (Fig. 6) varies very much with

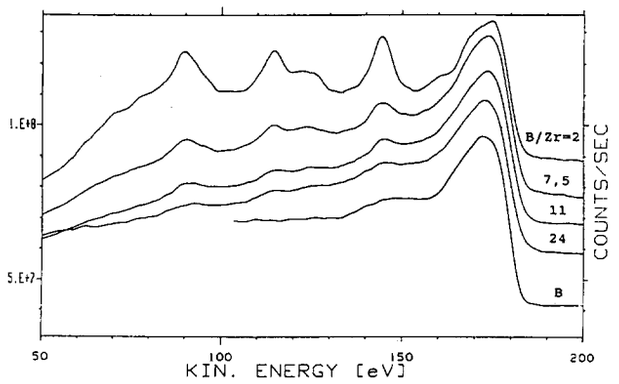

Fig. 12. AES spectra for different composition deposits. Boron *KLL* transition.

the experimental conditions. The emerging grain facets are either hexagonal, and then representative of the (001) planes, or rectangular, corresponding to the (100), (010) and (110) planes.

It was also observed that the pyramidal crystallites are given by the (*hkl*) planes with $h = k > 0$ and $l > 0$. The grain size can reach 15 μm.

The largest crystals, up to 30 μm, were obtained in the domain Ω for the oriented type I growth.

The codeposition of free boron radically modifies the deposit morphologies (Fig. 9(c)). They present an aspect of 'cauliflower', generally characteristic of amorphous products. This phenomenon is particularly clear when it goes from monophase domain ZrB_2 to biphasic domain $ZrB_2(i) + B$. The deposits are very well crystallized, only the presence of the boron considerably lowers the crystallite size, which is emphasized in the biphasic domain $ZrB_2(III) + B$.

The aspect of amorphous deposits (Fig. 13) in the domain B(a) is different from latter one's by a metallic aspect and by a negligible roughness.

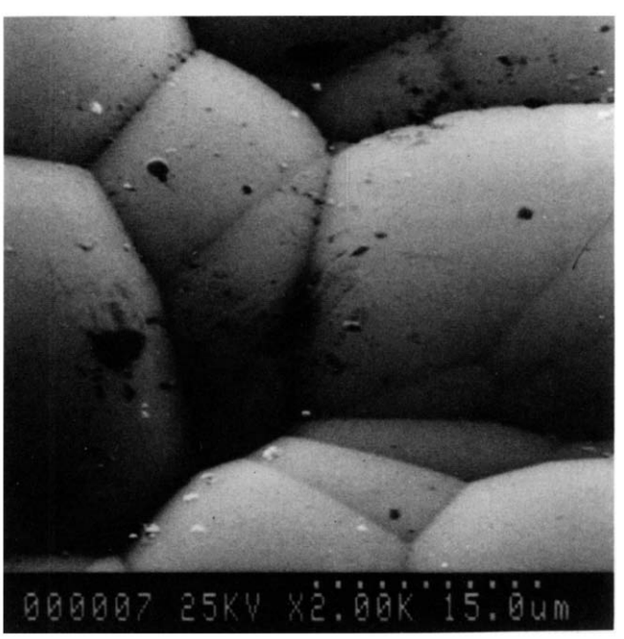

Fig. 13. Surface morphology of amorphous deposits.

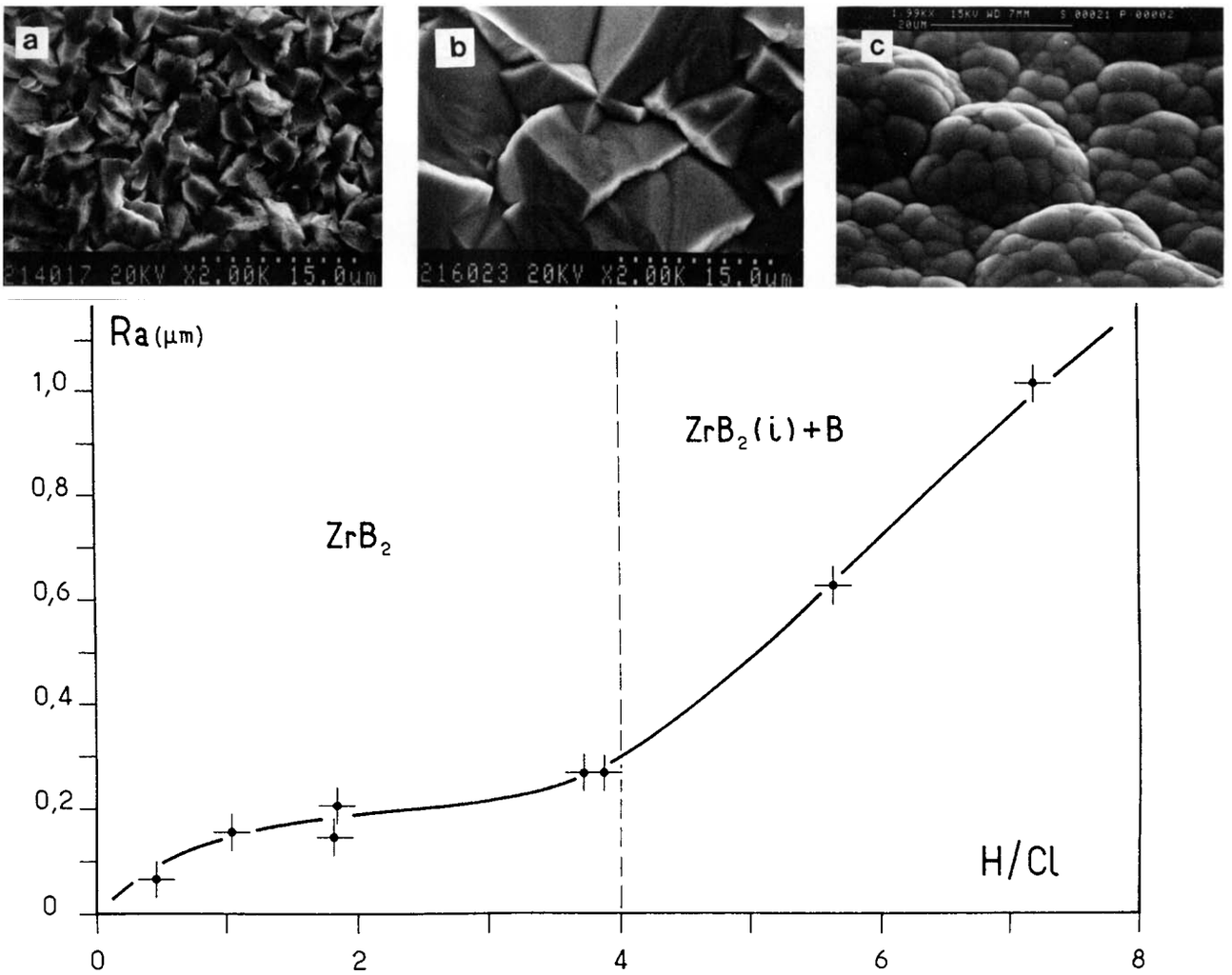

Fig. 14. Effect of hydrogen concentration on rugosity (*Ra*) and morphology. $T = 1373$ K, $P_T = 10^3$ Pa, B/Zr = 6. (a) H/Cl = 0·46; (b) H/Cl = 3·73; (c) H/Cl = 7·2.

The various aspects of the layer surface have been quantified, as a function of the main parameter, by measuring the roughness (*Ra*).

Even though the parameter domain has been widened, in agreement with the results given by the experimental design, a temperature change from 1080 K to 1480 K does not have an influence on the roughness.

In contrast, the influence of the hydrogen concentration is very important. Figure 14 shows that the roughness (*Ra*) of the deposit surface and the crystal size (Fig. 14(a) and (b)) increases with H/Cl ratio in the monophasic domain. It tends to be stabilized in crossing the Ω domain ($1 < H/Cl < 4$).

The rising part of the curve corresponds to the aspect 'cauliflower' in domain $ZrB_2(i) + B$ (Fig. 14(c)). The agglomeration becomes more and more voluminous when the hydrogen concentration increases, but the crystallite size decreases.

The positive influence of the pressure increase on the deposition rate is, here in the Ω domain, shown by the rapid crystal growth (Fig. 15). It confirms the results from the experimental design. Under the same deposition conditions, the arithmetic rugosity (*Ra*) varies from 0·21 μm for the deposit obtained at 10 mbar to 1·6 μm for those obtained at 50 mbar.

5.5 Microhardness

The Vickers hardness has been measured with an automated microhardness meter. The measurement has been realized on the surface and on sections of the deposited layer which were polished with diamond paste to 1 μm.

Figure 16 gives the hardness variation versus the composition (B/Zr) with 100 g load. In the ZrB_2 monophasic domain, the microhardness varies from 21·5 to 26 GPa. These values are in agreement with those determined by other authors ($H_{v150} = 23{\cdot}3$ GPa for sintered material,[13,14] $H_{v25} = 22$ GPa for vapour-deposited products[5]).

It seems that the hardness has little sensitivity to microstructure. There is not any difference between the measurements performed on the surface and on the section of the deposits with type I orientation.

Contrary to the results of Gebhardt & Cree,[5] the hardness increases with boron content and becomes

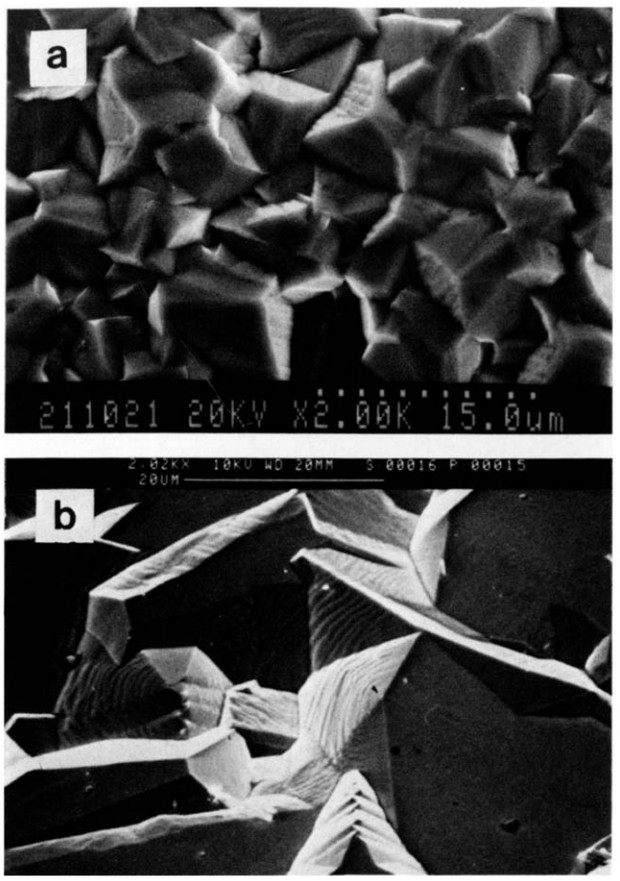

Fig. 15. Effect of reaction pressure on crystalline size. $T=$ 1373 K, $BCl_3/ZrCl_4 = 6$, $H/Cl = 1{\cdot}8$. (a) $P_T = 10^3$ Pa; (b) $P_T = 5 \times 10^3$ Pa.

constant around 31 GPa for the B/Zr ratio superior to 11 (boron excess >65 vol.%).

A more rigorous characterization of a material's resistance to the penetration of an indenter consists of determining the constants k and n of the Meyer relation ($P = kd^n$) between the load (P) and the imprint diagonal (d).

Figure 17 shows the linearization of the Meyer law for the deposits of different compositions.

The index (n) varies with the boron content in the solid, but the constant k, more directly related to the material properties, varies in the same way with boron content.

For pure diboride (B/Zr = 2) (with $k = 1{\cdot}9758$ and $n = 1{\cdot}7976$, P in g, d in μm) the hardness can be calculated thanks to the relation $H_v(\text{kg.mm}^{-2}) = 3956P^{-0{\cdot}1126}$, for any load P, if the indenter is in the form of Vickers pyramid.

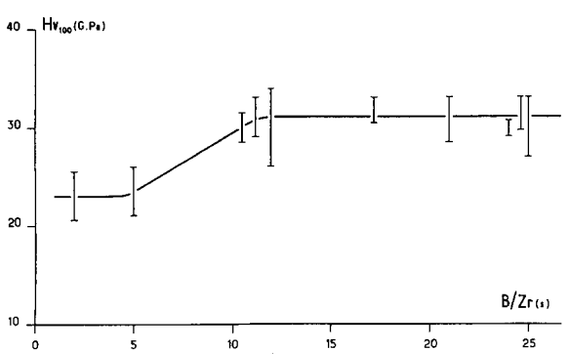

Fig. 16. Microhardness versus deposit composition.

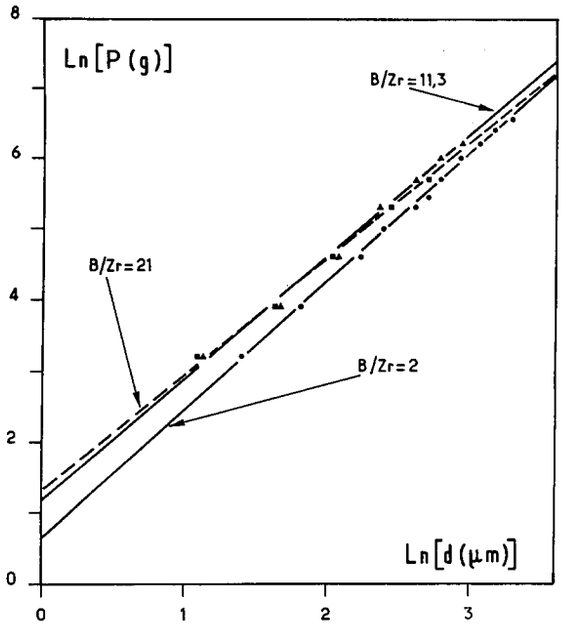

Fig. 17. Meyer constants for various composition deposits.

6 Discussion and Conclusion

An important aspect of this system is that the experimental results are in good agreement with the thermodynamic prediction.[9] It seems to prove that the system is experimentally approaching equilibrium.

The influence of the parameters on the system is generally identical in these two cases. The observed differences are caused by the hydrodynamic diffusion and reaction phenomena in the gaseous phase or the crystalline growth, which, in addition to the surface reaction, contribute to the whole deposition process.

It is particularly true in the case of pressure variations. In fact, the augmentation of total pressure increases the deposition rate, but, according to the theoretical analysis, the yield of solid phases would be diminished. So it is thought that pressure will have more influence on the concentration gradient in the boundary layer (positive effect on the system) than on the surface reaction (negative effect).

In the same manner, the maximum deposition rate is situated at a temperature (1450 K) inferior to the theoretical temperature (1730 K) for the maximum yield. This shift can be due to the existence of homogeneous reactions which are different from that producing the high-temperature species (subchlorides, C, H) predicted by thermodynamics.

Also the above-mentioned phenomenon can be

the cause of the displacement of the frontiers in the experimental diagram compared to the theoretical diagram. In this case the poor sensitivity of the characterization methods (principally the X-ray diffraction) can have an effect.

Compared with the theoretical curve, the deposition rate decrease with BCl_3 rising concentration is emphasized. That could result from microstructure changes (decrease of the crystallite size) when free boron is codeposited with diboride.

Moreover, in the explored temperature range, the obtained results show that BCl_3 reduction by hydrogen has a strong influence on the chemical system.

However, there exist two kinetic mechanisms below and above 1170 K. At low temperature the deposit growth can be limited by the homogeneous reaction

$$BCl_3 + H_2 \rightarrow BCl_2H + HCl \qquad (1)$$

or by the heterogeneous reaction

$$BCl_3 + 3/2H_2 \rightarrow B + 3HCl \qquad (2)$$

In the thermodynamic approach, it was concluded that the homogeneous reaction (1) is the most probable. The diboride or the free boron is formed from the intermediate species BCl_2H. In fact, the formation of zirconium diboride from the elements or directly from the chlorides is less probable in this system.

Above the transition temperature the process is generally controlled by the diffusion of the gaseous species in the boundary layer, which is, for a large part, constituted of hydrogen. It is thought that the diffusion of this molecule is the limiting step.

Acknowledgements

The authors wish to thank R: Berjoan, F. Sibieude and R. Flamand (Institut de Science et de Génie des Matériaux et des Procédés, Odeillo, 66120 Font-Romeu, France) for participating in the characterization of deposits, as well as the SEP (Société Europeenne de Propulsion, le Haillan, 33165 Saint Medard en Jalles, France) for supporting this work.

References

1. Moers, K., Methods for preparation of high-melting carbides, nitrides and borides, and description of a few of their properties: II. *Z. Anorg. Allgem. Chem.*, **198** (1931) 243–61.
2. Randich, E., Chemical vapor-deposited borides of the form $(Ti,Zr)B_2$ and $(Ta,Ti)B_2$. *Thin Solid Films*, **63** (1979) 309–13.
3. Motojima, S., Funahashi, K. & Kurosawa, K., ZrB_2 coated on copper plate by chemical vapour deposition and its corrosion and oxidation stabilities. *Thin Solid Films*, **189** (1990) 73–9.
4. Takahashi, T. & Kamiya, H., Chemical vapor deposition of the system Ti–Zr–B. *High Temperatures–High Pressures*, **9** (1977) 437–43.
5. Gebhardt, J. J. & Cree, R. F., Vapor-deposited borides of group IVA metals. *J. Am. Ceram. Soc.*, **48** (1965) 262–7.
6. Rice, G. W. & Woodin, R. L., Zirconium borohydride as a zirconium boride precursor. *J. Am. Ceram. Soc.*, **71** (1988) C-181–C-183.
7. Feichtner, J. D. & Veligdan, J. T., Procédé de revêtement d'un substrat par décomposition thermique d'un composé métallique. US Patent 2 567 542, 1986.
8. Domrachev, G. A., Vapour phase deposition of inorganic coatings. UK Patent 1 306 784, 1973.
9. Wang, A. & Male, G., Thermodynamics of the heterogeneous system $ZrCl_4$–BCl_3–H_2. *Calphad*, **16** (1992) 229–40.
10. Feneuille, D., Mathieu, D. & Phan-Tan-Luu, R., Méthodologie de la recherche expérimentale. Univ. Aix-Marseille, pers. comm., 1977.
11. Wallace, C. A. & Ward, R. C. C., An X-ray cylindrical texture camera for the examination of thin films. *J. Appl. Cryst.*, **8** (1975) 255–60.
12. Vandenbulcke, L. & Vuillard, G., Polymorphism in boron deposition by the H_2 reduction of BCl_3. *J. Less-Common Metals*, **67** (1979) 65–78.
13. Ordan'Yan, S. S., Dmitriev, A. I., Bizhev, K. T. & Stepanenko, E. K., Interaction in the system B_4C–ZrB_2. *Sov. Powder Metall. Met. Ceram.* (Engl. transl.), **27** (1988) 38–40.
14. Meyer, R. & Pastor, H., Les borures réfractaires: étude particulière des borures de titane et de zirconium; préparation, propriétés et applications. *Bull. Soc. Français de Céram.*, **66** (1965) 59–80.